ACS APPLIED MATERIALS & INTERFACES

Research Article

www.acsami.org

Surface-Functionalized Porous Lignin for Fast and Efficient Lead Removal from Aqueous Solution

Zhili Li,[†,‡] Duo Xiao,[†] Yuanyuan Ge,*[,†] and Stephan Koehler[‡]

[†]School of Chemistry and Chemical Engineering, Guangxi University, Nanning, 530004, China

[‡]School of Engineering and Applied Sciences, Harvard University, Cambridge, Massachusetts 02138, United States

Supporting Information

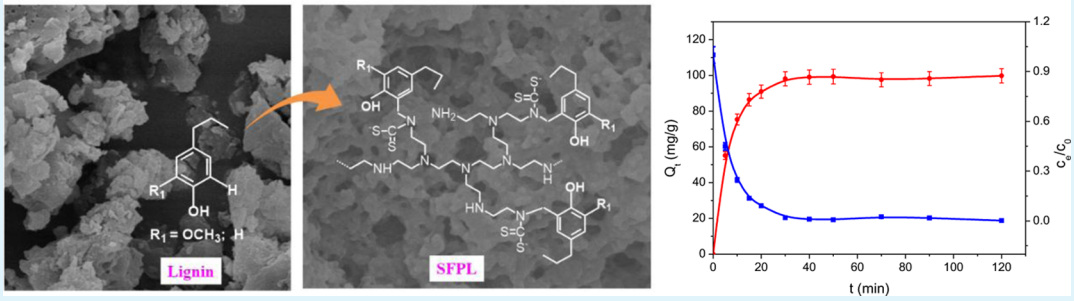

ABSTRACT: The development of ecofriendly sorbents for fast and efficient removal of heavy metals from aqueous media still remains a significant challenge. Here, we report that this task can be addressed by creating a porous naturally occurring polymer, as illustrated by functionalizing lignin with large numbers of mesopores and functional groups. We show that surface-functionalized porous lignin (SFPL), obtained by a two-step process, has a large surface area of 22.3 m^2/g, 12 times that of lignin, and a high density of dithiocarbamate groups (2.8 mmol/g). SFPL was found to exhibit an excellent adsorption performance toward lead ions dissolved in water. For example, 99% of the lead ions from 50 mL of a solution containing 20 mg/L lead ions was removed in just 30 min by 0.01 g of SFPL. The saturated adsorption capacity of SFPL for lead ions was found to be 188 mg/g, which is 13 times that of the original lignin and 7 times that of activated carbon. The adsorption process is endothermic and involves intraparticle diffusion and chemical adsorption between lead ions and the functional groups of SFPL. The cost effectiveness and environmental friendliness of SFPL make it a promising material for removing lead and other heavy metals from wastewater.

KEYWORDS: *lignin, porous, surface functionalization, lead, adsorption*

1. INTRODUCTION

Water pollution by heavy metals poses a major environmental threat because these elements tend to bioaccumulate and cause ecological damage.[1] To minimize the amount of heavy metals released into the environment, the development of high-performance sorbents is an essential pursuit for industrial applications and environmental remediation. Porous silica,[2] porous carbon,[3,4] porous metal−organic frameworks (MOFs),[5,6] and porous gels[7,8] have all been investigated for the remediation of heavy metals from aqueous solution thanks to their high surface areas and high stabilities. Currently, research into cost-effective and ecofriendly sorbents concerning structure design, synthesis methods, and intriguing properties has been widely carried out. Biomass materials, such as cellulose, lignin, chitosan, and agricultural wastes, have attracted a great deal of attention for heavy-metal removal on account of their natural abundance, low cost, biocompatibility, and low environmental impact.[9−12]

Lignin is the second most abundant biomass on Earth after cellulose.[13] It is commonly generated as a byproduct from the pulp and paper industry and is considered as a waste.[13] Lignin is a complex, amorphous natural polymer containing phenolic hydroxyl, methoxyl, and ether groups, which have a low ability to adsorb metal ions.[14,15] More recently, progressive results obtained by introducing additional functional groups such as amine, sulfonic, and xanthate groups onto the lignin matrix were obtained by our group.[12,16,17] Unfortunately, low adsorption rates and low adsorption capacities significantly diminished the practical usage of all of these lignin-based sorbents. The ideal adsorbent must contain a high porosity, large surface area, and strong binding-site accessibility for adsorbates to achieve both rapid adsorption and a high adsorption capacity.[18,19] However, to date, porous lignin-based materials containing strong binding sites for heavy metals have yet to be synthesized.

In this work, we developed a cost-effective and environmentally safe two-step process for synthesizing surface-functionalized porous lignin (SFPL) with strong dithiocarba-

Received: May 8, 2015
Accepted: June 22, 2015
Published: June 22, 2015

DOI: 10.1021/acsami.5b03994
ACS Appl. Mater. Interfaces 2015, 7, 15000−15009

Scheme 1. Two-Step Synthesis Process of SFPL from Lignin, PEI, and Carbon Disulfide: (a) Mannich reaction, (b) Esterification[a]

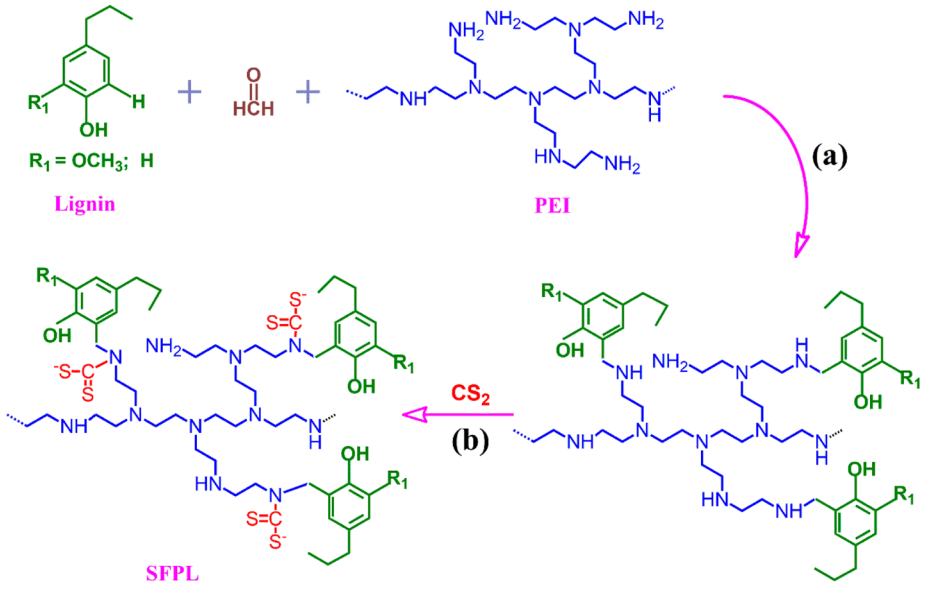

[a]Lignin, green; dithiocarbamate, red; PEI, blue.

mate and amine/imine functional groups from an alkaline lignin, a byproduct of the pulp and paper industry, for the removal of heavy metals from aqueous solution. We used a Mannich reaction[20] to graft polyethylenimine (PEI) onto an alkaline lignin matrix (Scheme 1a). PEI is a highly branched polymer that contains many primary/secondary amine groups, which can be esterified with CS_2 to introduce dithiocarbamate groups[21] (Scheme 1b) and form a porous structure. Although there have been a few reports on PEI incorporation into silica materials and metal−organic frameworks[22−24] developed for CO_2 separation, to the best of our knowledge, the incorporation of branched PEI into lignin for heavy-metal capture is unprecedented. We thus expect that the PEI-grafted lignin dithiocarbamate composite will provide a large surface area with many pores for interacting with heavy-metal ions. Furthermore, numerous amine/imine and dithiocarbamate functional groups on this ecofriendly biopolymer can strongly chelate with heavy-metal ions,[25] which should increase the capacity and rate of heavy-metal ions adsorption. Among various heavy metals, lead has been recognized as one of the most toxic. Because of its high toxicity and damage to the kidneys, liver, nervous system, and reproductive system,[26] lead must be thoroughly removed from the environment. Therefore, we chose lead as a model heavy metal to investigate the adsorption performance of SFPL. The effects of several operating parameters, such as solution pH, adsorbent dosage, contact time, initial ion concentration, and temperature, on the adsorption of lead by SFPL were investigated. Kinetic models were used to identify the possible mechanisms of the adsorption process. The Langmuir and Freundlich models were also used to analyze the adsorption equilibrium isotherms.

2. EXPERIMENTAL SECTION

2.1. Materials. Alkaline lignin was obtained by precipitation from black liquor (Nanpu Pulp Mill, Nanning, China) with H_2SO_4 at pH 2.0. Polyethylenimine [PEI, M_w = 7000 Da, 50 wt % aqueous solution, $(C_2H_5N)_n$, N content = 32.56 wt %], copper nitrate, lead nitrate, cadmium nitrate, nickel nitrate, and zinc nitrate were purchased from Aladdin Co. Ltd., Beijing, China. Carbon disulfide, formaldehyde, sodium hydroxide, and hydrochloric acid were purchased from Shantou Xilong Chemicals Ltd., Shantou, China, and were all of reagent grade. Metal nitrates were dissolved in deionized water as metal-ion solution samples. Deionized water from a Milli-Q Plus water purification system (Millipore) was used throughout the experiments.

2.2. Synthesis of SFPL. SFPL was synthesized by a two-step method. In a typical experiment, 2.0 g of alkaline lignin, 4.0 g of PEI solution, and 150 mL of deionized water were added to a 250 mL three-neck flask, and the mixture was continuously stirred for 30 min. Eight milliliters of formaldehyde was added dropwise to this mixture, and then the temperature was raised to 90 °C for 5 h to enable the Mannich reaction (Scheme 1a). After that, the mixture was cooled to 40 °C, 10 mL of carbon disulfide was added dropwise into the flask, and the mixture was kept for 2 h to complete the esterification (Scheme 1b). Finally, the mixture was filtered and washed with ethanol and deionized water several times. After drying drying the filtrate in a vacuum at 50 °C for 24 h, we collected a red-brown powder, namely, SFPL.

2.3. Characterizations. Elemental analysis for C, H, N, and S in SFPL was performed on a PE 2400 II Element Analyzer. Fourier transform infrared (FTIR) spectra were recorded on a Nexus 470 spectrometer using the KBr pellet method and scanning the range between 400 and 4000 cm^{-1}. Morphological measurements were recorded by field-emission scanning electron microscopy (SEM, SU8020, Hitachi). X-ray photoelectron spectroscopy (XPS) was performed on a Kratos Axis Ultra DLD X-ray photoelectron spectrometer using monochromatic Al Kα (1486.6 eV) X-rays and an analytical chamber with a base pressure of 10^{-9} Torr. Nitrogen adsorption isotherms were measured with a Micromeritics Gemini VII 2390 Instrument. Before the measurements, the samples were degassed in a vacuum at 373 K for 12 h. The Brunauer−Emmett−Teller (BET)[27] method was utilized to calculate the specific surface areas (S_{BET}, m^2/g) from the N_2 adsorption isotherm in the relative pressure range of p/p_0 = 0.05−0.3. The total pore volume (V_p, cm^3/g) was calculated at p/p_0 = 0.99. The average pore size (d_p, nm) was determined as $d_p = 4V_p/S_{BET}$.

2.4. Batch Adsorption Studies. Batch adsorption was performed in conical flasks with magnetic stirring at 100 rpm to guarantee good dispersion. The flasks were placed in a water bath at 25 ± 0.5 °C for a suitable contact time (t = 180 min except for kinetic adsorption) to allow complete equilibration [initial metal-ion concentration (c_0) =

DOI: 10.1021/acsami.5b03994
ACS Appl. Mater. Interfaces 2015, 7, 15000−15009

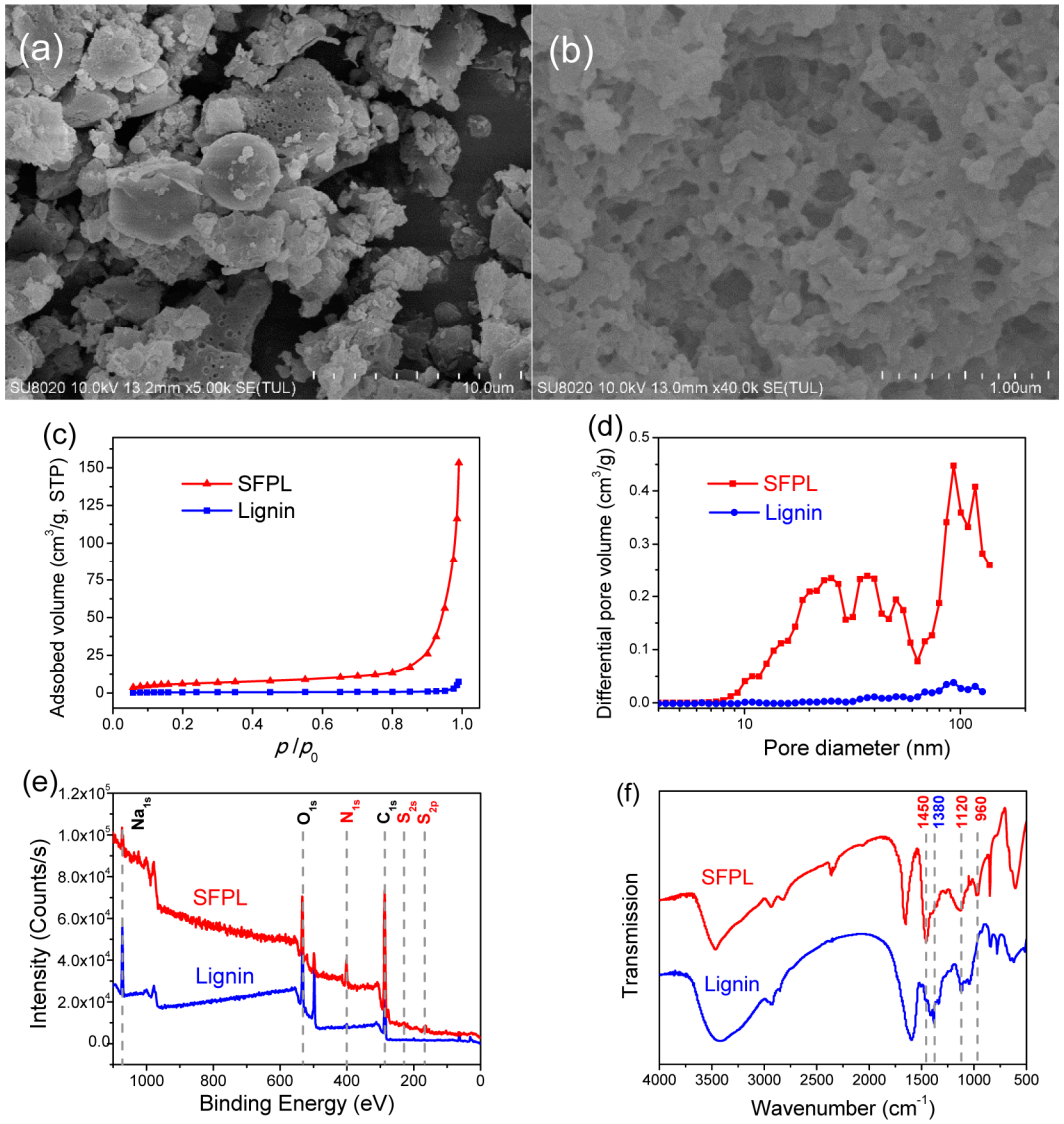

Figure 1. (a,b) SEM images of (a) lignin and (b) SFPL and (c) nitrogen adsorption isotherms, (d) pore diameter distributions, (e) XPS spectra, and (f) FTIR spectra of lignin and SFPL.

10−110 mg/L, adsorbent dosage = 0.01 g/50 mL, pH = 5]. The pH value of the solution was adjusted with 0.1 mol/L HCl or NaOH. We varied the SFPL dosages for solutions with an initial metal-ion concentration of 20 mg/L to determine the influence of dosage on adsorption. Kinetic adsorption was conducted at a lead-ion concentration of 20 mg/L, pH 5, with an SFPL dosage of 0.01 g/50 mL. At predetermined time intervals, the solutions were pipetted from the conical flask and filtered for concentration detection. At the end of each experiment, the solutions were separated by filtration using 0.22-μm-pore-size filters. The filtrate was analyzed for residual lead ions by inductively coupled plasma optical emission spectrometry (ICP-OES, Optima 5300DV, Perkin-Elmer), with a plasma gas flow of 15 L/min and a nebulizer gas flow of 0.6 L/min. The pump rate was 100 rpm, and the sample uptake rate was 1.2 mL/min for 30 s. The wavelengths for Cd, Cu, Zn, and Pb were 226.5, 324.7, 213.9, and 220.4 nm, respectively. All tests were conducted in triplicate, and their mean values were used in analyzing the data. The removal efficiency (E) and adsorption amount (Q_e) were calculated accordingly.

3. RESULTS AND DISCUSSION

3.1. Synthesis and Structural Characteristics of SFPL. SFPL was prepared by functionalization of lignin using a two-step process. In the first step, amine groups were attached to the lignin matrix through a Mannich reaction involving the active hydrogen near the phenolic hydroxyl group (Ph−OH) of lignin and PEI in the presence of a cross-linker, namely, formaldehyde. In the second step, the amine groups were reacted with carbon disulfide to produce SFPL with dithiocarbamate groups (as shown in Scheme 1). Both reactions are facile reactions.[28,29] In our efforts to develop a modified lignin with high efficiency for the adsorption of lead ions, we selected branched PEI as the grafting agent for both its high content of reactive primary/secondary amine groups and its high-branched structure.[21] We measured the N contents of the product to investigate the effects of the amounts of PEI and formaldehyde and the Mannich reaction temperature on the PEI loading; the results are presented in the Supporting Information (SI). Figure S1a (SI) shows the significant impact of the amount of PEI on the N content of SFPL. As the amount of PEI was increased, the N content definitely increased. However, when the amount of PEI was excessive, the side reaction with formaldehyde occurred,[20,30] and thus, no increase in N content was observed. Figure S1b (SI) reveals similar regulation for formaldehyde. The Mannich reaction temper-

DOI: 10.1021/acsami.5b03994
ACS Appl. Mater. Interfaces 2015, 7, 15000−15009

ature had a slight positive effect on the N content (Figure S1c, SI). Considering the endothermic nature of the Mannich reaction,[31] we chose 90 °C for the Mannich reaction. We also used the S content to evaluate the effect of the amount of carbon disulfide on the dithiocarbamate loading. As shown in Figure S1d (SI), with increasing carbon disulfide dosage, the S content increased. However, excess carbon disulfide evaporated because of its low boiling point (46 °C). Under these optimum reaction conditions, namely, 2.0 g of lignin, 2.0 g of PEI, 8 mL of formaldehyde, and 10 mL of CS_2, the prepared SFPL contained 46.91% carbon, 11.97% nitrogen, 5.92% hydrogen, and 17.93% sulfur, determined by elemental analysis. It was calculated that the total contents of nitrogen and dithiocarbamate groups in SFPL were around 8.5 and 2.8 mmol/g, respectively. This means about 32.9% of the amine groups were converted into dithiocarbamate groups. Considering that N comes from PEI whereas S comes from CS_2, it was also calculated that the PEI and carbon disulfide loadings in SFPL were about 36.76% and 21.29%, respectively. It should be noted that the development of SFPL is a good residual utilization of lignin and that the synthetic route does not produce any waste; the overdosed carbon disulfide and formaldehyde used in the process can be collected by ice-cooled condensers and reused. Therefore, this method is a simple and environmentally friendly route for synthesizing surface-functional lignin materials.

SEM micrographs showed that SFPL contained considerable mesopores (Figure 1b), whereas the original alkaline lignin was in the form of flocks without pores (Figure 1a). This is due to the grafting of highly branched PEI on lignin, which benefited the formation of pores and an increase in the surface area of SFPL. Fifty pores were picked from the SEM image, and their form factors were analyzed with ImageJ, version 1.48v.[32] As shown in Figure S2 (SI), these pores had an average form factor of 0.72 (where a value of 1.0 indicates a perfect circle). The BET surface area and pore diameter distribution of SFPL were further analyzed by N_2 adsorption isotherms. The results are reported in Figure 1c,d and Table 1. The N_2 adsorption isotherm of SFPL can be classified as type III according to the IUPAC classification. The increase in the nitrogen adsorption of SFPL at a high relative pressure above 0.9 might arise in part from the mesopores and macropores associated with the interparticulate voids.[33] The BET surface area of SFPL calculated over a relative pressure (p/p_0) range from 0.05 to 0.3 was found to be 22.3 m^2/g, which is 12 times that of lignin (S_{BET} = 1.8 m^2/g). The pore diameter distribution curve of SFPL (Figure 1d) and the average pore size of SFPL (d_p = 41.3 nm) calculated using density functional theory (DFT)[34] further suggest the presence of mesopores and macropores. Moreover, SFPL exhibited a much larger total pore volume (0.23 cm^3/g) than lignin (V_p = 0.01 cm^3/g). In contrast, lignin showed a nonporous structure according to the N_2 adsorption isotherm and pore size distribution curve (Figure 1c,d). The increases in the BET surface area and total pore volume of alkaline lignin confirm that a porous structure was successfully introduced, which will benefit the adsorption of lead ions from aqueous solution.

Table 1. Textural Properties of Lignin and SFPL

	S_{BET} (m^2/g)	V_p (cm^3/g)	d_p (nm)
lignin	1.8	0.01	25.3
SFPL	22.3	0.23	41.3

To confirm that the —NCSS$^-$ group was attached to SFPL during surface treatment of alkaline lignin, we obtained XPS and FTIR spectra. XPS measurements of lignin and SFPL showed that the surface treatment introduced nitrogen and sulfur. We observed three additional peaks having binding energies of 162 eV (S 2p), 226 eV (S 2s), and 399.5 eV (N 1s), confirming the presence of sulfur and nitrogen,[35] as shown in Figure 1e. FTIR measurements further confirmed the attachment of these two elements and also showed their bonding configurations, as shown in Figure 1f. Compared with lignin, SFPL exhibited additional FTIR absorption peaks at 1120 and 960 cm^{-1} that can be assigned to the stretching vibrations of C═S and C—S bonds, respectively, within the —NCSS$^-$ functional group.[36] Moreover, the peak associated with C—N stretching vibrations shifted to 1450 cm^{-1} for SFPL, because of the neighboring C═S double bond.[35] The band at 1380 cm^{-1} is due to C—O stretching. We thus conclude that the surface treatment transferred the —NCSS$^-$ group to SFPL.

3.2. Effect of pH on Pb(II) Adsorption by SFPL. We measured the lead adsorption by SFPL at different pH values ranging from 2 to 6 with an initial lead-ion concentration of 20 mg/L at 25 ± 0.5 °C, an SFPL dosage of 0.01 g/50 mL, and a contact time of 180 min. As shown in Figure 2a, the uptake of lead ions was strongly affected by the solution pH. The adsorption efficiency was low, ~50%, at pH 2 but increased to ~99% at pH 5. At low pH, excess protons in aqueous solution

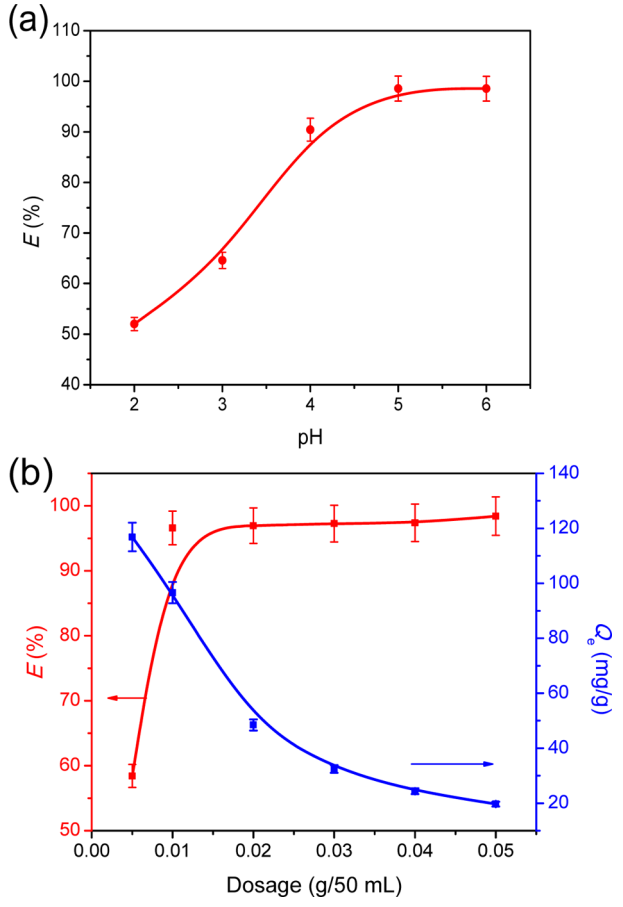

Figure 2. Dependence of the adsorption efficiency on (a) pH [c_0 = 20 mg/L, SFPL dosage = 0.01 g/50 mL, temperature (T) = 25 ± 0.5 °C, t = 180 min] and (b) SFPL dosage (c_0 = 20 mg/L, pH = 5, T = 25 ± 0.5 °C, t = 180 min).

DOI: 10.1021/acsami.5b03994
ACS Appl. Mater. Interfaces 2015, 7, 15000−15009

can compete with heavy-metal ions for the available active sites. At the same time, the functional groups (amine/imine and dithiocarbamate groups on SFPL) are protonated, that is, the sorbents surface carry more positive charges at lower pH values.[37] When the initial pH is increased from 2 to 5, the amine/imine and dithiocarbamate groups gradually become deprotonated; hence greatly enhancing lead-ion adsorption efficiency. Moreover, lead hydroxide precipitation will occur as pH > 6.[35] Therefore, to eliminate the effect of the precipitation of metal hydroxides, further adsorption of lead ions was conducted at pH 5.

3.3. Effect of SFPL Dosage on Pb(II) Adsorption. We also measured the adsorption of lead ions as a function of SFPL dosage at pH 5 for an initial concentration of 20 mg/L at a temperature of 25 ± 0.5 °C for a contact time of 180 min. As shown in Figure 2b (left axis), the removal of lead increased sharply from 57% to 99% when the adsorbent loading was increased from 0.005 to 0.01 g/50 mL (corresponding to an increase in the liquid-to-solid ratio from 10000:1 to 5000:1), which can be attributed to an increase in the number of active adsorption sites.[38] When the dosage was continuously increased to 0.05 g/50 mL, the lead removal efficiency increased slightly. In parallel, the absorption amount decreased from 120 to 20 mg/g with increasing SFPL dosage, as shown in Figure 2b (right axis). This is due to the decrease of the ratio of adsorbate to adsorbent. As the initial lead-ion content was constant, the amount of lead ions adsorbed per unit mass decreased with increasing SFPL dosage. Therefore, the optimal adsorbent dosage for the investigation of adsorption was selected as 0.01 g/50 mL for the subsequent experiments.

3.4. Effect of Contact Time on Pb(II) Adsorption by SFPL. To determine the absorption kinetics, we measured the amount of lead ions adsorbed by SFPL at a lead-ion concentration of 20 mg/L, a pH of 5, an SFPL dosage of 0.01 g/50 mL, and a temperature of 25 ± 0.5 °C. A sharp increase in lead adsorption occurred in the first 15 min, followed by a slow adsorption process, as shown in Figure 3a. In fact, 91% of the lead was adsorbed in the initial 20 min. After 30 min of exposure, saturation was achieved, and almost 99% of the lead ions had been removed by SFPL (Figure 3a, right axis). The adsorption rate was higher than those of other lead-adsorbing materials including carbon nanotubes and activated carbon (as listed in Table 2). The fast adsorption of lead ions by SFPL is due largely to the porous structure and the large number of functional groups on SFPL that can interact with lead ions.

We used pseudo-first-order[45] and pseudo-second-order[46] models, as well as the intraparticle diffusion model,[47] to analyze the experimental kinetic data according to the following linear equations

Pseudo-first-order model

$$\log(Q_e - Q_t) = \log Q_e - \left(\frac{k_1 t}{2.303}\right) \quad (1)$$

Pseudo-second-order model

$$\frac{t}{Q_t} = \frac{1}{k_2 Q_e^2} + \frac{1}{Q_e} t \quad (2)$$

Intraparticle diffusion model

$$Q_t = k_{int} t^{1/2} + \theta \quad (3)$$

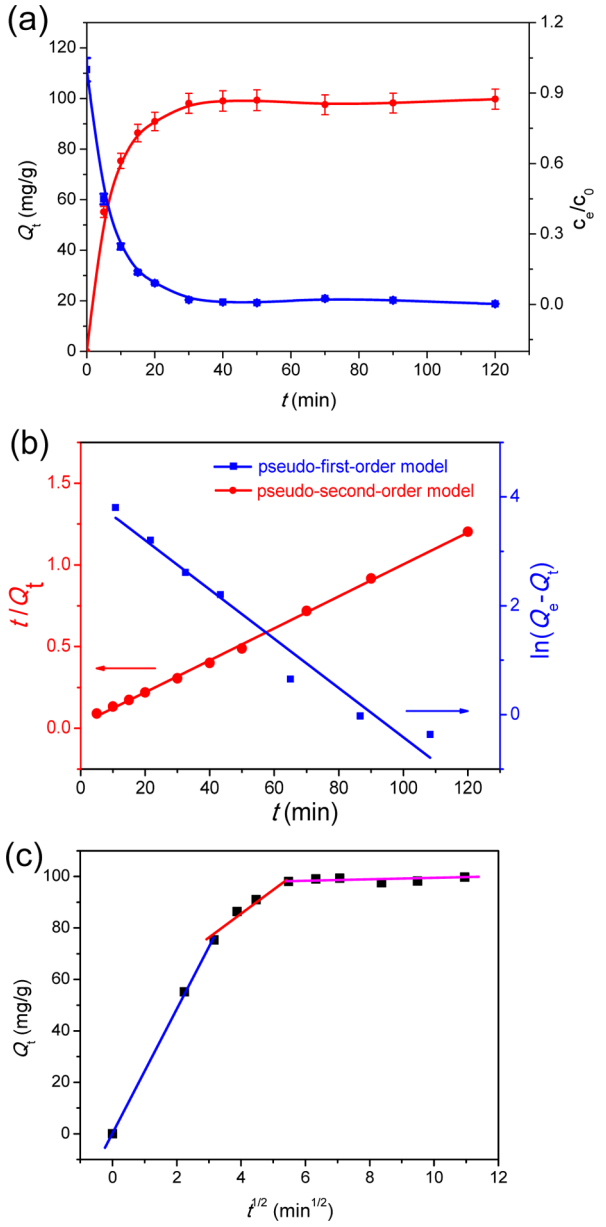

Figure 3. (a) Adsorption kinetics of lead on SFPL (c_0 = 20 mg/L, SFPL dosage = 0.01 g/50 mL, pH = 5, T = 25 ± 0.5 °C). (b) Fitting results for pseudo-first-order and pseudo-second-order models. (c) Plots of lead adsorption on SFPL according to the intraparticle diffusion model.

where k_1 (1/min) is the pseudo-first-order rate constant; k_2 [g/(mg·min)] is the pseudo-second-order kinetic rate constant; k_{int} [mg/(g·min$^{1/2}$)] is a constant related to the diffusion coefficient; θ is the intercept for the intraparticle diffusion model; and Q_e and Q_t are the amounts (mg/g) of the metal ions adsorbed at equilibrium and at contact time t (min), respectively. Lines obtained in plots of these expressions with linear regression coefficients (R^2) indicate the applicability of the pseudo-first-order and the pseudo-second-order models for fitting the adsorption process (Figure 3b). The correlation coefficients of the pseudo-first-order and pseudo-second-order equations for the adsorption of Pb(II) ions are given in Table 3. A comparison of the correlation coefficients of the two equations for Pb(II) adsorption indicates that the pseudo-second-order model (R^2 = 0.9985) is better able to describe the

DOI: 10.1021/acsami.5b03994
ACS Appl. Mater. Interfaces 2015, 7, 15000−15009

Table 2. Comparison of Pb(II) Uptake on SFPL and Other Adsorbents

adsorbent	equilibrium time (min)	adsorption capacity (mg/g)	ref
glycerol-modified lignin	240	9	39
modified soda lignin	60	46	40
amine-modified lignin	60	61	20
lignin xanthate	90	62	12
carbon nanotube	240	101	41
acidified carbon nanotube	360	91	42
silica gel	40	83	43
activated carbon	105	27	44
SFPL	30	188	present study

Table 3. Adsorption Kinetics Fitting Results for Lead Ions on SFPL by Pseudo-First-Order, Pseudo-Second-Order, and Intraparticle Diffusion Models

Pseudo-First-Order Model		
Q_e (mg/g)	k_2 (1/min)	R^2
60.3	0.097	0.9600
Pseudo-Second-Order Model		
Q_e (mg/g)	k_2 [g/(mg·min)]	R^2
102	0.0039	0.9985
Intraparticle Diffusion Model		
θ	k_{int}	R^2
40.8	7.3	0.5802

adsorption behavior over the whole range of adsorption. The pseudo-second-order model assumes that the rate-limiting step of adsorption is a chemisorption between the metal ions and the binding sites of the adsorbent.[35] Therefore, it can be inferred that the adsorption of Pb(II) on SFPL is mainly controlled by the chemical interaction between SFPL and lead ions. According to hard−soft acid−base (HSAB) theory,[48] lead is a Lewis soft acid that can react with Lewis soft bases, such as amine/imine and dithiocarbamate groups, through covalent bonds.

The kinetic results were also analyzed using the intraparticle diffusion model. According to this model, if the so-called Weber−Morris[49] plot of Q_t versus $t^{1/2}$ is a straight line that passes through the origin, then the adsorption process is controlled by intraparticle diffusion alone. However, if the data exhibit multilinear plots, then two or more steps influence the sorption process.[50] As shown in Figure 3c, the plot was correlated by three straight lines: The first straight portion represents the external resistance to mass transfer surrounding the particles, which involves the movement of lead ions from the bulk solution to the solid phase; the second linear portion represents the intraparticle diffusion of lead ions into the mesopores and macropores; and the third linear portion represents equilibrium adsorption, where the rate of adsorption decareses because of the low adsorbate content in the bulk solution. Because the plot does not pass through the origin (θ = 40.8), intraparticle diffusion is not the only rate-limiting step.[51] These findings suggest that the adsorption of lead ions on SFPL involves complex mechanisms, including intraparticle diffusion and chemisorption.

3.5. Effect of Initial Lead Concentration on Pb(II) Adsorption by SFPL. To obtain the adsorption capacity of SFPL for lead ions, we measured adsorption isotherms for a range of initial lead concentrations at pH 5, for an SFPL dosage of 0.01 g/50 mL, a temperature of 25 ± 0.5 °C, and a contact time of 180 min. Alkaline lignin was used as a reference. The adsorption capacity increased with increasing initial lead concentration, as shown in Figure 4a. This increase in the

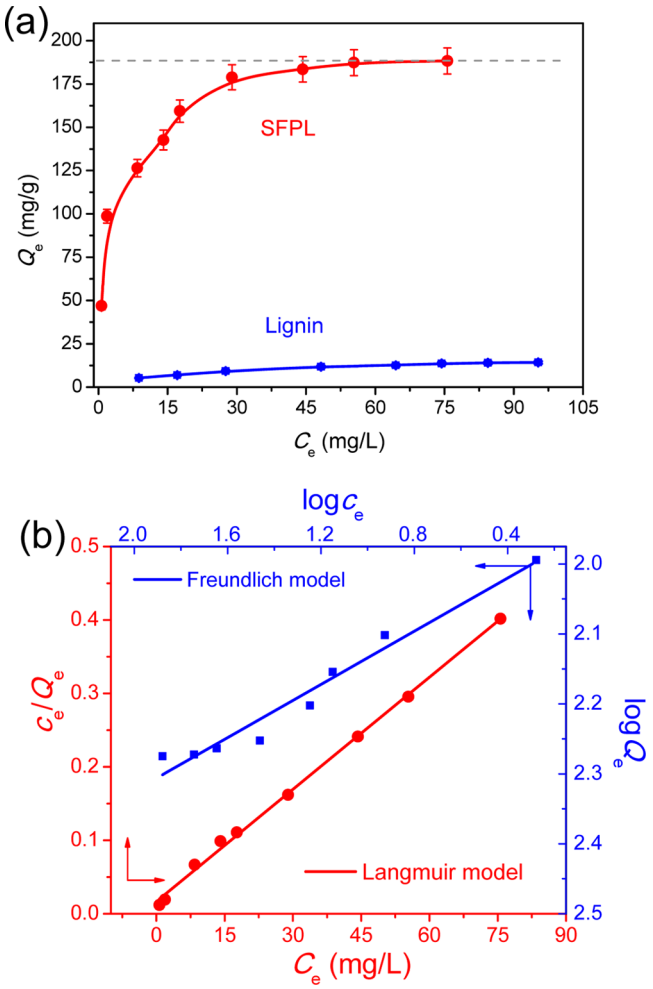

Figure 4. (a) Adsorption isotherms of lead on SFPL (SFPL dosage = 0.01 g/50 mL, pH = 5, T = 25 ± 0.5 °C, t = 180 min) with lignin as a reference. (b) Fitting results for the Langmuir and Freundlich isotherm models.

loading capacity of SFPL is due to the fact that the higher the lead concentration, the greater the number of active adsorption sites of SFPL involved, and thus the larger the adsorption amount. The saturated adsorption capacity of Pb(II) on SFPL was found to be 188 mg/g, which is 13 times that on lignin (14.3 mg/g). SFPL also showed a much higher adsorption capacity for lead ions than other lead-adsorbing materials, including carbon nanotubes (2 times), activated carbon (7 times), and silica gels (2 times), as reported in Table 2. The high adsorption capacity of SFPL for lead is due to its porous structure and surface-attached dithiocarbamate and amine/imine groups.

We used the Langmuir isotherm model to fit our experimental data, which is based on the assumption that adsorption occurs through monolayer sorption onto a surface

DOI: 10.1021/acsami.5b03994
ACS Appl. Mater. Interfaces 2015, 7, 15000−15009

with a finite number of homogeneous sites.[52] It can be described by the linear equation

$$\frac{1}{Q_e} = \frac{1}{Q_m} + \frac{1}{bQ_mC_e} \quad (4)$$

where Q_m is the maximum adsorption capacity (mg/g), C_e is the final equilibrium lead concentration, and b is the Langmuir constant (L/mg). The adsorption capacity is in good agreement with the Langmuir adsorption model (R^2 = 0.9975), as shown in Figure 4b and Table 4. The adsorption

Table 4. Langmuir and Freundlich Model Fitting Parameters for Lead-Ion Adsorption on SFPL[a]

Langmuir Model		
Q_m (mg/g)	b (L/mg)	R^2
200	0.005	0.9975
Freundlich Model		
K_F	n	R^2
87.9	5.26	0.9582

[a]Experimental saturation amount Q_e = 188 mg/g.

capacity (Q_m = 200 mg/g) is in accordance with the experimental saturation amount (Q_e = 188 mg/g), which indicates that the SFPL surface is homogeneous and that the adsorption can be characterized as monolayer adsorption.[52] The Freundlich isotherm model was also used to analysis the adsorption data. The Freundlich model, which assumes a heterogeneous adsorbing surface and active sites, is given by the linear expression[53]

$$\log Q_e = \log K_F + \frac{1}{n} \log C_e \quad (5)$$

where K_F is a constant related to the adsorption capacity (mg/g) (L/mg)$^{1/n}$ and n is an empirical parameter related to the adsorption intensity. Compared with that of the Langmuir model, the low correlation coefficient (R^2 = 0.9582) of the Freundlich model indicates that it is in poor agreement with the experimental data, as shown in Table 4 and Figure 4b.

3.6. Effect of Temperature on Pb(II) Adsorption by SFPL. To investigate the effect of temperature on the adsorption process, different temperatures of 25, 40, and 55 °C were used to obtain the amount of Pb(II) adsorbed by SFPL at c_0 = 40 mg/L, SFPL dosage = 0.01 g/50 mL, pH = 5, and t = 180 min. The standard Gibbs free energy change ($\Delta G°$), standard enthalpy change ($\Delta H°$), and standard entropy change ($\Delta S°$) were determined according to the equations[54]

$$\Delta G° = -RT \ln k_d \quad (6)$$

$$\ln k_d = -\frac{\Delta H°}{RT} + \frac{\Delta S°}{R} \quad (7)$$

where k_d is the distribution coefficient and R is the gas constant [J/(mol·K)].

The effect of temperature on the adsorption of Pb(II) by SFPL is shown in Figure 5a. As the temperature was increased from 25 to 40 and 55 °C, the amount of Pb(II) adsorbed by SFPL increased from 143 to 156 and 169 mg/g, respectively. The probable reason for this behavior is that the diffusion rate of the sorbate within the pores increased and the solution viscosity decreased as the temperature was increased, thereby causing an increase in the frequency of collisions between SFPL and lead ions[55] and thus enhancing the adsorption amount. From the plots of the distribution coefficient k_d versus temperature in Figure 5b, it can be seen that k_d increased with increasing temperature, an indication of adsorption that is endothermic in nature.[12] According to eq 7, the values of $\Delta H°$ and $\Delta S°$ were calculated from the slope and intercept, respectively, of a plot of ln k_d versus $1/T$. The calculated values of thermodynamic parameters are presented in Table 5.

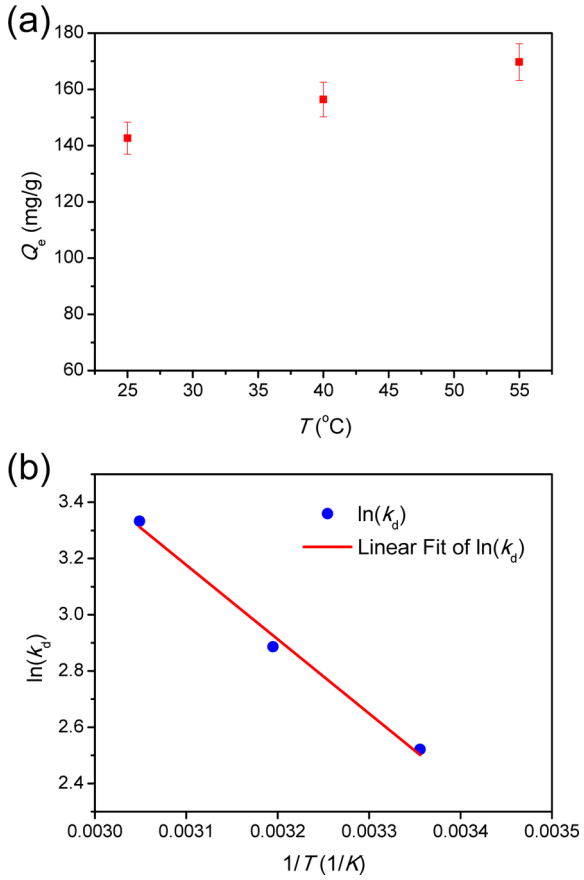

Figure 5. (a) Effect of temperature on the adsorption of Pb(II) by SFPL (c_0 = 40 mg/L, SFPL dosage = 0.01 g/50 mL, pH = 5, t = 180 min). (b) Plot of ln k_d versus $1/T$ for the adsorption of Pb(II) by SFPL.

Table 5. Thermodynamic Parameters for the Adsorption of Pb(II) by SFPL

T (1/K)	$\Delta G°$ (kJ/mol)	$\Delta H°$ (kJ/mol)	$\Delta S°$ (J/K mol)
298	−6.2	21.9	94.4
313	−7.5		
328	−9.1		

The overall Gibbs free energy changes during the adsorption process at 25, 40, and 55 °C were found to be negative, indicating spontaneous adsorption of Pb(II) onto SFPL. The increase in the absolute value of $\Delta G°$ with increasing temperature indicates that the adsorption process becomes more favorable at higher temperature.[56] The positive value of the enthalpy change ($\Delta H°$ = 21.9 kJ/mol) indicates that the adsorption is endothermic in nature.[57] The positive value of the entropy change ($\Delta S°$ = 94.4 J/K mol) suggests that the randomness at the solid−solution interface increases during the adsorption of Pb(II) on SFPL.[58]

DOI: 10.1021/acsami.5b03994
ACS Appl. Mater. Interfaces 2015, 7, 15000−15009

3.7. Comparison Adsorption of Heavy Metals by SFPL. Solutions separately containing Cu(II), Cd(II), Ni(II), Zn(II), and Pb(II) (each 100 mg/L, pH 5) were prepared. To 50 mL of each of these solutions was added 0.01 g of SFPL, and the mixture was stirred for 180 min. After that, the amounts of these metals adsorbed by SFPL were calculated. The adsorption results are presented in Figure 6. It was found that the

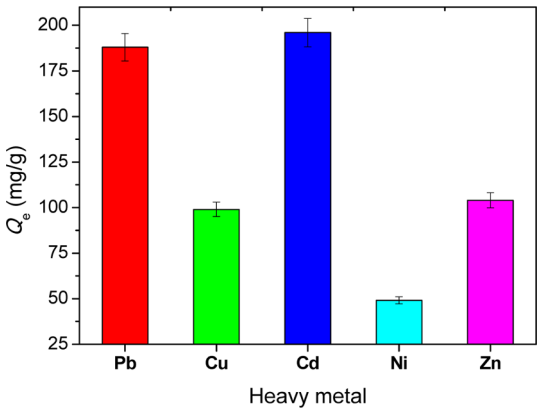

Figure 6. Comparative adsorption of Pb(II) and other heavy metals by SFPL.

equilibrium adsorption amounts, Q_e, of Cd(II) and Pb(II) were much higher than those of the other metals, with an ordering of Cd(II) > Pb(II) > Zn(II) > Cu(II) > Ni(II), indicating that SFPL has an obvious adsorption selectivity to Cd(II) and Pb(II). Both the characteristics of the functional groups on SFPL and the properties of the metal ions should be taken into consideration to account for the adsorption selectivity. According to HSAB theory,[48] as Lewis soft acids, cadmium and lead ions have precedence over zinc, copper, and nickel ions, which can be regarded as middle-soft acids, in interactions with the amine/imine and dithiocarbamate groups of SFPL, which are Lewis soft bases.[59] Thus, SFPL shows a stronger covalent affinity to Cd(II) and Pb(II), compared to weaker interactions with Cu(II), Zn(II), and Ni(II).

3.8. Adsorption Mechanism of Pb(II) by SFPL. The high adsorption rate and high adsorption capacity of Pb(II) on SFPL can be clarified as follows: First, as is well-known, PEI carries large amounts of amine and imine functional groups. After being esterified with carbon disulfide, SFPL has plenty of additional functional groups, namely, dithiocarbamate groups. The sulfur and nitrogen coexisting functional groups are expected to have a strong affinity to Pb(II) ions from aqueous solutions.[20,60] It is reasonable that these functional groups can provide sufficient active adsorption sites to form strong complexes with Pb(II) on the SFPL surface and thereby enhance the adsorption capacity of Pb(II). Second, the grafting of highly branched PEI on lignin increases the specific surface area and total pore volume of SFPL, increases the interaction areas between the sorbent and adsorbate, and accordingly effectively enhances the adsorption rate and capacity of Pb(II) ions. In addition, there are abundant ether and phenolic units on the lignin chains, which could also form complexes with Pb(II) in aqueous solution.[14,61] The synergistic effects of these functional groups, the large surface area, and the numerous mesopores certainly play a key role in the adsorption.

Given that alkali lignin is the main organic ingredient present in black liquor from the pulp and paper industry that has not yet been converted into high-value products on a large scale and that today is mainly used for energy recovery at pulp mills, the preparation of SFPL from alkaline lignin for lead removal from aqueous solution provides significant advantages of wide availability, high value-added, fast and efficient adsorption, and environmental friendliness compared to other sorbents, such as carbon nanotubes and activated carbon. The lignin structure is highly dependent on the source and delignification process,[62] and the active hydrogen near Ph−OH might be occupied by a methoxy group, making it hard for the Mannich reaction to take place. Fortunately, demethoxylation can be accomplished by enzymes,[63] fungi,[64] thermal treatment,[65] and hydrotreating.[66] Thus, suitable pretreatments (demethoxylation, degradation, etc.) for different lignins are essential to achieve the production of surface-functional porous lignin (SFPL) with similar properties and yields.

4. CONCLUSIONS

We have reported a surface-functionalized porous lignin (SFPL) material synthesized by a two-step process and successfully introduced dithiocarbamate functional groups (2.8 mmol/g). The material had a high BET surface area (22.3 m^2/g) with a large number of mesopores (41.3 nm). Compared to other lead-adsorbing materials, SFPL was found to have a high lead adsorption capacity (Q_e = 188 mg/g) with a high adsorption rate (t = 30 min). The kinetics of lead adsorption by SFPL can be well-described by a pseudo-second-order model, which indicates a chemical interaction between lead ions and SFPL. The adsorption isotherm was found to be well-fit by the Langmuir model. According to the values of thermodynamic parameters, namely, ΔH° and ΔG°, the adsorption of lead by SFPL is an endothermic and spontaneous process. The effectiveness of SFPL is due to its high porosity, its large surface area, and the high affinity of lead ions to dithiocarbamate and amine/imine groups. Moreover, because lignin is a renewable biomass obtained as a byproduct from the pulp and paper industry, the manufacture of SFPL from lignin is both cost-effective and environmentally friendly. SFPL exhibits great potential for treating wastewater containing toxic heavy-metal ions.

■ ASSOCIATED CONTENT

Ⓢ Supporting Information

Figures indicating the influences of the synthetic parameters on the N and S contents of SFPL, form factor distribution of SFPL determined with ImageJ, version 1.48v. The Supporting Information is available free of charge on the ACS Publications website at DOI: 10.1021/acsami.5b03994.

■ AUTHOR INFORMATION

Corresponding Author

*E-mail: geyy@gxu.edu.cn.

Notes

The authors declare no competing financial interest.

■ ACKNOWLEDGMENTS

We acknowledge the support from the National Natural Science Foundation of China (Nos. 21264002, 21464002).

DOI: 10.1021/acsami.5b03994
ACS Appl. Mater. Interfaces 2015, 7, 15000−15009

REFERENCES

(1) Schwarzenbach, R. P.; Escher, B. I.; Fenner, K.; Hofstetter, T. B.; Johnson, C. A.; von Gunten, U.; Wehrli, B. The Challenge of Micropollutants in Aquatic Systems. *Science* **2006**, *313*, 1072−1077.

(2) Sangvanich, T.; Sukwarotwat, V.; Wiacek, R. J.; Grudzien, R. M.; Fryxell, G. E.; Addleman, R. S.; Timchalk, C.; Yantasee, W. Selective Capture of Cesium and Thallium from Natural Waters and Simulated Wastes with Copper Ferrocyanide Functionalized Mesoporous Silica. *J. Hazard. Mater.* **2010**, *182*, 225−231.

(3) Shin, Y. S.; Fryxell, G.; Um, W. Y.; Parker, K.; Mattigod, S. V.; Skaggs, R. Sulfur-Functionalized Mesoporous Carbon. *Adv. Funct. Mater.* **2007**, *17*, 2897−2901.

(4) Musico, Y. L. F.; Santos, C. M.; Dalida, M. L. P.; Rodrigues, D. F. Improved Removal of Lead(II) from Water Using a Polymer-Based Graphene Oxide Nanocomposite. *J. Mater. Chem. A* **2013**, *1*, 3789−3796.

(5) Khan, N. A.; Hasan, Z.; Jhung, S. H. Adsorptive Removal of Hazardous Materials Using Metal−Organic Frameworks (MOFs): A Review. *J. Hazard. Mater.* **2013**, *244*, 444−456.

(6) Abney, C. W.; Gilhula, J. C.; Lu, K.; Lin, W. Metal−Organic Framework Templated Inorganic Sorbents for Rapid and Efficient Extraction of Heavy Metals. *Adv. Mater.* **2014**, *26*, 7993−+.

(7) Bag, S.; Trikalitis, P. N.; Chupas, P. J.; Armatas, G. S.; Kanatzidis, M. G. Porous Semiconducting Gels and Aerogels from Chalcogenide Clusters. *Science* **2007**, *317*, 490−493.

(8) Tavares, D. S.; Daniel-da-Silva, A. L.; Lopes, C. B.; Silva, N. J. O.; Amaral, V. S.; Rocha, J.; Pereira, E.; Trindade, T. Efficient Sorbents Based on Magnetite Coated with Siliceous Hybrid Shells for Removal of Mercury Ions. *J. Mater. Chem. A* **2013**, *1*, 8134−8143.

(9) Farooq, U.; Kozinski, J. A.; Khan, M. A.; Athar, M. Biosorption of Heavy Metal Ions Using Wheat Based Biosorbents—A Review of the Recent Literature. *Bioresour. Technol.* **2010**, *101*, 5043−5053.

(10) Miretzky, P.; Cirelli, A. F. Cr(VI) and Cr(III) Removal from Aqueous Solution by Raw and Modified Lignocellulosic Materials: A Review. *J. Hazard. Mater.* **2010**, *180*, 1−19.

(11) Hubbe, M. A.; Hasan, S. H.; Ducoste, J. J. Cellulosic Substrates for Removal of Pollutants from Aqueous Systems: A Review. 1. Metals. *Bioresources* **2011**, *6*, 2161−U2914.

(12) Li, Z.; Kong, Y.; Ge, Y. Synthesis of Porous Lignin Xanthate Resin for Pb^{2+} Removal from Aqueous Solution. *Chem. Eng. J.* **2015**, *270*, 229−234.

(13) Laurichesse, S.; Avérous, L. Chemical Modification of Lignins: Towards Biobased Polymers. *Prog. Polym. Sci.* **2014**, *39*, 1266−1290.

(14) Albadarin, A. B.; Al-Muhtaseb, A. H.; Al-laqtah, N. A.; Walker, G. M.; Allen, S. J.; Ahmad, M. Biosorption of Toxic Chromium from Aqueous Phase by Lignin: Mechanism, Effect of Other Metal Ions and Salts. *Chem. Eng. J.* **2011**, *169*, 20−30.

(15) Brdar, M.; Šćiban, M.; Takači, A.; Došenović, T. Comparison of Two and Three Parameters Adsorption Isotherm for Cr(VI) onto Kraft Lignin. *Chem. Eng. J.* **2012**, 108−111.

(16) Ge, Y.; Li, Z.; Kong, Y.; Song, Q.; Wang, K. Heavy Metal Ions Retention by Bi-Functionalized Lignin: Synthesis, Applications, and Adsorption Mechanisms. *J. Ind. Eng. Chem.* **2014**, *6*, 4429−4436.

(17) Li, Z.; Xiao, D.; Kong, Y.; Ge, Y. Enhancing Lead Adsorption Capacity by Controlling the Chain Length of Alkyl Amine Grafted Lignin. *Bioresources* **2015**, *10*, 2425−2432.

(18) Deze, E. G.; Papageorgiou, S. K.; Favvas, E. P.; Katsaros, F. K. Porous Alginate Aerogel Beads for Effective and Rapid Heavy Metal Sorption from Aqueous Solutions: Effect of Porosity in Cu^{2+} and Cd^{2+} Ion Sorption. *Chem. Eng. J.* **2012**, *209*, 537−546.

(19) Chen, J. H.; Hsu, K. C.; Chang, Y. M. Surface Modification of Hydrophobic Resin with Tricaprylmethylammonium Chloride for the Removal of Trace Hexavalent Chromium. *Ind. Eng. Chem. Res.* **2013**, *52*, 11685−11694.

(20) Ge, Y.; Song, Q.; Li, Z. A Mannich Base Biosorbent Derived from Alkaline Lignin for Lead Removal from Aqueous Solution. *J. Ind. Eng. Chem.* **2015**, *23*, 228−234.

(21) Li, Z. L. Synthesis of a Carbamide-Based Dithiocarbamate Chelator for the Removal of Heavy Metal Ions from Aqueous Solutions. *J. Ind. Eng. Chem.* **2014**, *20*, 586−590.

(22) Kuwahara, Y.; Kang, D.-Y.; Copeland, J. R.; Brunelli, N. A.; Didas, S. A.; Bollini, P.; Sievers, C.; Kamegawa, T.; Yamashita, H.; Jones, C. W. Dramatic Enhancement of CO_2 Uptake by Poly(ethyleneimine) Using Zirconosilicate Supports. *J. Am. Chem. Soc.* **2012**, *134*, 10757−10760.

(23) Goeppert, A.; Czaun, M.; May, R. B.; Prakash, G. K. S.; Olah, G. A.; Narayanan, S. R. Carbon Dioxide Capture from the Air Using a Polyamine Based Regenerable Solid Adsorbent. *J. Am. Chem. Soc.* **2011**, *133*, 20164−20167.

(24) Jiang, D.; Burrows, A. D.; Xiong, Y.; Edler, K. J. Facile Synthesis of Crack-Free Metal−Organic Framework Films on Alumina by a Dip-Coating Route in the Presence of Polyethylenimine. *J. Mater. Chem. A* **2013**, *1*, 5497−5500.

(25) Farrukh, A.; Akram, A.; Ghaffar, A.; Hanif, S.; Hamid, A.; Duran, H.; Yameen, B. Design of Polymer-Brush-Grafted Magnetic Nanoparticles for Highly Efficient Water Remediation. *ACS Appl. Mater. Interfaces* **2013**, *5*, 3784−3793.

(26) Jarup, L. Hazards of Heavy Metal Contamination. *Br. Med. Bull.* **2003**, *68*, 167−182.

(27) Brunauer, S.; Emmett, P. H.; Teller, E. Adsorption of Gases in Multimolecular Layers. *J. Am. Chem. Soc.* **1938**, *60*, 309−319.

(28) Pramanik, M.; Bhaumik, A. Phosphonic Acid Functionalized Ordered Mesoporous Material: A New and Ecofriendly Catalyst for One-Pot Multicomponent Biginelli Reaction under Solvent-Free Conditions. *ACS Appl. Mater. Interfaces* **2014**, *6*, 933−941.

(29) Pinheiro, P. C.; Tavares, D. S.; Daniel-da-Silva, A. L.; Lopes, C. B.; Pereira, E.; Araújo, J. P.; Sousa, C. T.; Trindade, T. Ferromagnetic Sorbents Based on Nickel Nanowires for Efficient Uptake of Mercury from Water. *ACS Appl. Mater. Interfaces* **2014**, *6*, 8274−8280.

(30) Córdova, A.; Watanabe, S.-i.; Tanaka, F.; Notz, W.; Barbas, C. F. A Highly Enantioselective Route to Either Enantiomer of Both α- and β-Amino Acid Derivatives. *J. Am. Chem. Soc.* **2002**, *124*, 1866−1867.

(31) Mitsumori, S.; Zhang, H.; Ha-Yeon Cheong, P.; Houk, K. N.; Tanaka, F.; Barbas, C. F. Direct Asymmetric Anti-Mannich-Type Reactions Catalyzed by a Designed Amino Acid. *J. Am. Chem. Soc.* **2006**, *128*, 1040−1041.

(32) Schneider, C. A.; Rasband, W. S.; Eliceiri, K. W. NIH Image to ImageJ: 25 Years of Image Analysis. *Nat. Methods* **2012**, *9*, 671−675.

(33) Lippens, B. C.; Linsen, B. G.; Deboer, J. H. Studies on Pore Systems in Catalysts I. The Adsorption of Nitrogen; Apparatus and Calculation. *J. Catal.* **1964**, *3*, 32−37.

(34) Olivier, J. P.; Conklin, W. B.; Szombathely, M. v. Determination of Pore Size Distribution from Density Functional Theory: A Comparison of Nitrogen and Argon Results. *Stud. Surf. Sci. Catal.* **1994**, *87*, 81−89.

(35) Ge, Y.; Xiao, D.; Li, Z.; Cui, X. Dithiocarbamate Functionalized Lignin for Efficient Removal of Metallic Ions and the Usage of the Metal-Loaded Bio-Sorbents as Potential Free Radical Scavengers. *J. Mater. Chem. A* **2014**, *2*, 2136−2145.

(36) Desseyn, H. O.; Fabretti, A. C.; Forghieri, F.; Preti, C. Isotopic Infrared Study of Some Nickel(II) and Copper(II) Complexes Containing Heterocyclic Dithiocarbamate Ligands. *Spectrochim. Acta A* **1985**, *41*, 1105−1108.

(37) Taty-Costodes, V. C.; Fauduet, H.; Porte, C.; Delacroix, A. Removal of Cd(II) and Pb(II) Ions, from Aqueous Solutions, by Adsorption onto Sawdust of *Pinus sylvestris*. *J. Hazard. Mater.* **2003**, *105*, 121−142.

(38) Bansal, M.; Singh, D.; Garg, V. K. A Comparative Study for the Removal of Hexavalent Chromium from Aqueous Solution by Agriculture Wastes' Carbons. *J. Hazard. Mater.* **2009**, *171*, 83−92.

(39) Demirbas, A. Adsorption of Lead and Cadmium Ions in Aqueous Solutions onto Modified Lignin from Alkali Glycerol Delignication. *J. Hazard. Mater.* **2004**, *109*, 221−226.

(40) Ibrahim, M. N. M.; Ngah, W. S. W.; Norliyana, M. S.; Daud, W. R. W.; Rafatullah, M.; Sulaiman, O.; Hashim, R. A Novel Agricultural

DOI: 10.1021/acsami.5b03994
ACS Appl. Mater. Interfaces 2015, 7, 15000−15009

Waste Adsorbent for the Removal of Lead(II) Ions from Aqueous Solutions. *J. Hazard. Mater.* **2010**, *182*, 377−385.
(41) Tofighy, M. A.; Mohammadi, T. Adsorption of Divalent Heavy Metal Ions from Water Using Carbon Nanotube Sheets. *J. Hazard. Mater.* **2011**, *185*, 140−147.
(42) Wang, H.; Zhou, A.; Peng, F.; Yu, H.; Yang, J. Mechanism Study on Adsorption of Acidified Multiwalled Carbon Nanotubes to Pb(II). *J. Colloid Interface Sci.* **2007**, *316*, 277−283.
(43) Ghoul, M.; Bacquet, M.; Morcellet, M. Uptake of Heavy Metals from Synthetic Aqueous Solutions Using Modified PEI—Silica Gels. *Water Res.* **2003**, *37*, 729−734.
(44) Sekar, M.; Sakthi, V.; Rengaraj, S. Kinetics and Equilibrium Adsorption Study of Lead(II) onto Activated Carbon Prepared from Coconut Shell. *J. Colloid Interface Sci.* **2004**, *279*, 307−313.
(45) Azizian, S. Kinetic Models of Sorption: A Theoretical Analysis. *J. Colloid Interface Sci.* **2004**, *276*, 47−52.
(46) Ho, Y.-S. Review of Second-Order Models for Adsorption Systems. *J. Hazard. Mater.* **2006**, *136*, 681−689.
(47) Annadurai, G.; Juang, R. S.; Lee, D. J. Use of Cellulose-Based Wastes for Adsorption of Dyes from Aqueous Solutions. *J. Hazard. Mater.* **2002**, *92*, 263−274.
(48) Pearson, R. G. Hard and Soft Acids and Bases. *J. Am. Chem. Soc.* **1963**, *85*, 3533−3539.
(49) Weber, W. J.; Morris, J. C. Kinetics of Adsorption on Carbon from Solution. *J. Sanit. Eng. Div., Am. Soc. Civ. Eng.* **1963**, *89*, 31−60.
(50) Sengil, I. A.; Ozacar, M. Biosorption of Cu(II) from Aqueous Solutions by Mimosa Tannin Gel. *J. Hazard. Mater.* **2008**, *157*, 277−285.
(51) Olu-Owolabi, B. I.; Diagboya, P. N.; Adebowale, K. O. Evaluation of Pyrene Sorption−Desorption on Tropical Soils. *J. Environ. Manage.* **2014**, *137*, 1−9.
(52) Langmuir, I. The Adsorption of Gases on Plane Surfaces of Glass, Mica and Platinum. *J. Am. Chem. Soc.* **1918**, *40*, 1361−1403.
(53) Freundlich, H. M. F. Over the Adsorption in Solution. *J. Phys. Chem.* **1906**, *57*, 385−470.
(54) Liu, Y. Is the Free Energy Change of Adsorption Correctly Calculated? *J. Chem. Eng. Data* **2009**, *54*, 1981−1985.
(55) Argun, M. E.; Dursun, S.; Ozdemir, C.; Karatas, M. Heavy Metal Adsorption by Modified Oak Sawdust: Thermodynamics and Kinetics. *J. Hazard. Mater.* **2007**, *141*, 77−85.
(56) Corrie, A. M.; Williams, D. R. Thermodynamic Considerations in Co-ordination. Part XXIV. Gibbs Free-Energy Changes, Enthalpies, and Entropies of Formation of Complexes of Glycinate, Glycylglycinate, Cysteinate, and Glutathionate with Hydrogen and Lead(II) Ions and Suggested Aqueous Structure. *J. Chem. Soc., Dalton Trans.* **1976**, 1068−1072.
(57) Eichler, B.; Zvara, I. Evaluation of the Enthalpy of Adsorption from Thermochromatographical Data. *Radiochim. Acta* **1982**, *30*, 233−238.
(58) Gök, Ö.; Özcan, A.; Erdem, B.; Özcan, A. S. Prediction of the Kinetics, Equilibrium and Thermodynamic Parameters of Adsorption of Copper(II) Ions onto 8-Hydroxy Quinoline Immobilized Bentonite. *Colloids Surf. A* **2008**, *317*, 174−185.
(59) Pearson, R. G. Hard and Soft Acids and Bases, HSAB, Part 1: Fundamental Principles. *J. Chem. Educ.* **1968**, *45*, 581.
(60) Say, R.; Birlik, E.; Erdemgil, Z.; Denizli, A.; Ersoz, A. Removal of Mercury Species with Dithiocarbamate-Anchored Polymer/Organosmectite Composites. *J. Hazard. Mater.* **2008**, *150*, 560−564.
(61) Mohan, D.; Pittman, C. U.; Steele, P. H. Single, Binary and Multi-Component Adsorption of Copper and Cadmium from Aqueous Solutions on Kraft Lignin—A Biosorbent. *J. Colloid Interface Sci.* **2006**, *297*, 489−504.
(62) Zakzeski, J.; Bruijnincx, P. C. A.; Jongerius, A. L.; Weckhuysen, B. M. The Catalytic Valorization of Lignin for the Production of Renewable Chemicals. *Chem. Rev.* **2010**, *110*, 3552−3599.
(63) Lopretti, M.; Cabella, D.; Morais, J.; Rodrigues, A. Demethoxylation of Lignin-Model Compounds with Enzyme Extracts from *Gloeophilum trabeum*. *Process. Biochem.* **1998**, *33*, 657−661.
(64) Niemenmaa, O.; Uusi-Rauva, A.; Hatakka, A. Demethoxylation of [$O^{14}CH_3$]-Labelled Lignin Model Compounds by the Brown-Rot Fungi *Gloeophyllum trabeum* and *Poria (Postia) placenta*. *Biodegradation* **2008**, *19*, 555−565.
(65) Asmadi, M.; Kawamoto, H.; Saka, S. Thermal Reactions of Guaiacol and Syringol as Lignin Model Aromatic Nuclei. *J. Anal. Appl. Pyrol.* **2011**, *92*, 88−98.
(66) Deutsch, K. L.; Shanks, B. H. Hydrodeoxygenation of Lignin Model Compounds over a Copper Chromite Catalyst. *Appl. Catal. A: Gen.* **2012**, *447*, 144−150.

DOI: 10.1021/acsami.5b03994
ACS Appl. Mater. Interfaces 2015, 7, 15000−15009